PAPER • OPEN ACCESS

High short-circuit current in PTB7-Th:ITIC organic solar cells induced by pulsed laser deposited MoO$_3$ layer

To cite this article: Godwin N Ugwuanyi *et al* 2025 *Nanotechnology* **36** 445401

View the article online for updates and enhancements.

High short-circuit current in PTB7-Th:ITIC organic solar cells induced by pulsed laser deposited MoO₃ layer

Godwin N Ugwuanyi[1] , Martin C Eze[1,2] , Sukhwinder Singh[1] , Hamed Ifheema[1],
Victoria G Rocha[3] , Bo Hou[4] and Gao Min[1,*]

[1] School of Engineering, Cardiff University, Cardiff CF24 3AA, United Kingdom
[2] School of Physics, University of Nigeria, Obukpa Rd, Nsukka, 410105 Enugu, Nigeria
[3] Instituto de Ciencia y Tecnologia del Carbono, INCAR-CSIC, C/Francisco Pintado Fe, 26, Oviedo
33011, Spain
[4] School of Physics, Cardiff University, Cardiff CF24 3AA, United Kingdom

E-mail: min@cardiff.ac.uk

CrossMark

Abstract

The paper reports a high short-circuit current density of 43.6 mA cm^{-2} obtained in an organic
solar cell (OSC) that has a device structure of indium-doped tin oxide/ZnO/PTB7-Th:ITIC/
MoO₃/Ag. The novel aspect of this work is that the MoO₃ layers were prepared using pulsed
laser deposition. The experimental data analysis indicates that the observed increase is
specifically associated with the pulsed laser deposited MoO₃ layers. Although the exact
mechanisms responsible for such huge increase are yet to be identified, the result of this work
shows that a significantly higher short-circuit current can be obtained in OSCs, offering a
potential pathway for further improving the power conversion efficiency of OSCs.

Supplementary material for this article is available online

1. Introduction

Organic solar cells (OSCs) are one of the emerging solar cell technologies that has enjoyed a significant advance in recent years. Since the invention of the bulk heterojunction (BHJ) architecture [1], the power conversion efficiency of OSCs has increased from approximately 1.0% in bilayer devices [2] in 1986 to over 6.0% in BHJ devices [3] in 2009. Ultrafast charge transfer between the semiconducting polymer and fullerene in self-assembled interpenetrating networks of two separated phases at 10–20 nm nanoscale is a key feature that facilitates the high efficiency of OSCs, which also offers an advantage of solution processibility toward low-cost manufacturing [1, 4]. Recently, advances in using non-fullerene acceptors to replace fullerene derivatives provide additional possibilities in spectrum absorption control and energy level alignment [5],

* Author to whom any correspondence should be addressed.

leading to steady increase in the power conversion efficiency of OSCs, now reaching 19% [6]. To date, numerous combinations between the polymer donors and non-fullerene accepters have been discovered; among these, the PTB7-Th:ITIC has been established as a promising BHJ architecture for OSCs due to its favourable molecule structure and energy band alignment [5, 7]. PTB7-Th is an intensively studied polymer donor [8], which mixes well with the ITIC acceptor [9, 10], exhibiting a sufficient gap between the HOMO and LOMO to enable a reasonably large Voc of 0.70–0.85 V [8, 11]. In addition to its advantages of being lightweight, non-toxic, printable and low-cost processability, the PTB7-Th:ITIC architecture has a high absorption coefficient, offering the possibility for making ultra-thin BHJ OSCs with potential for semitransparent applications [12].

To achieve adequate performance with some degree of transparency, it is crucial to ensure that both electron and hole transport layers are sufficiently transparent. ZnO, which has an energy bandgap of 3.4 eV, has been successfully demonstrated as an effective electron transport layer for many OSCs [13–15], while MoO_3 with an energy bandgap of approximately 3.0 eV has been investigated as a hole transport layer for several OSCs [16]. The common routes to prepare MoO_3 thin films are thermal evaporation [17–22] and solution processing [23, 24]. CVD and RF sputtering techniques have also been employed, due to their capability of controlling more deposition parameters [25, 26]. The preparation of MoO_3 thin films using the pulsed laser deposition (PLD) have also been reported [27, 28]. However, to date, pulsed laser deposited MoO_3 has not been used as a hole transport layer in OSCs. This is possibly due to a preconception that PLD involves energetic plumes of particles and high substrate temperature during growth [29, 30], which can cause damage to solution processed layers and consequently considered as an unfavourable technique in organic devices. On the other hand, considering that PLD is capable of stoichiometric transfer of the target material composition to the substrate and produce high quality thin films with flexible control, the novelty of this work is to explore the possibility of fabricating the high quality MoO_3 thin film as the hole transport layer using the PLD technique for the PTB7-Th:ITIC based semi-transparent OSCs.

With the MoO_3 as the hole transport layer, it was hoped that the shunt resistance and fill factor of the devices would be improved. Contrary to these expectations, the results of this work turned out to be the opposite—both the shunt resistance and fill factor were reduced, but surprisingly, an abnormally high short-circuit current density of 43.6 mA cm^{-2} was obtained. This is completely unexpected and potentially significant. Firstly, it adds further question to the recent debates on the roles of the MoO_3 as a hole transport layer in OSCs [16, 31]. Secondly, it provides experimental evidence, showing that the short-circuit current in OSCs can be higher than anticipated. The purpose of this paper is to report the key aspects of the experimental procedures that led to this unexpected higher short-circuit current density.

2. Materials and methods

Materials: The raw materials used in this study include: indium-doped tin oxide (ITO) glass of 1.1 mm thick with a sheet resistance of 7 Ω/□, purchased from Pingdingshan Mingshuo Technology Ltd, China; zinc acetate dihydrate (99.999% trace metals basis), 2-methoxyethanol (99.8% anhydrous), and ethanolamine (⩾99.5%) for the preparation of the zinc oxide (ZnO) electron transport layer, purchased from Sigma Aldrich UK; the PTB7-Th donor polymer (molecular weight of 153 000 g mol^{-1}) and the ITIC non-fullerene accepter (molecular weight of 1427.94 g mol^{-1}) for the preparation of the photoactive BHJ layers, was purchased from 1-Material Inc Canada; the chloroform (99.9% extra dry, stabilised, acro-seal) as a solvent, purchased from Fisher scientific UK; the molybdenum trioxide target (99.95%, 2 inch diameter, 0.125 inch thick) for the preparation of the hole transport layer by PLD, purchased from PI-KEM UK; the silver target (99.99%, 2 inch diameter, 0.125 inch thick) for the preparation of top electrode by magnetron sputtering, purchased from Kurt J. Lesker LTD UK; the dilute Hellmanex (III), acetone and isopropanol for cleaning, purchased from Sigma Aldrich UK and Fisher Scientific UK, respectively.

Device fabrication: The OSCs developed in this study are based on a device structure shown in figure 1, which consists of five layers in a form of ITO/ZnO/PTB7-Th:ITIC/MoO_3/Ag on a glass substrate. The fabrication started with a thorough cleaning of ITO/glass substrates (15 mm × 20 mm) using Hellmanex solution, rinsed with deionised water, sonicated in an ultrasonic bath using deionised water, acetone and isopropanol, respectively, dried by argon gas blow and treated in a UV-Ozone cleaner. Thereafter, the electron transport layer (ZnO) was deposited on the ITO by spin-coating at 5000 rpm for 30 s using 0.45 mol dm^{-3} of Zn(CH$_3$CO$_2$)$_2$.2H$_2$O solution, followed by annealing at 160 °C on a hot plate for 30 min. The photoactive layers were deposited on the ZnO layer by spin-coating at 5000 rpm for 30 s using 0.0051 mol dm^{-3} of the blended PTB7-Th:ITIC solution. All above processes were carried out in air with a relative humidity of 25%–55%. Subsequently, the MoO_3 hole transport layers were deposited on the freshly made photoactive layers by PLD (PLD2000, PVD products). All depositions were performed for 4 min using a 2 inch molybdenum trioxide disc target with the substrate temperature set at room temperature and the ablation rate at 18 Hz for different ablation energies of 140 mJ, 160 mJ, 180 mJ, 200 mJ, and 220 mJ, respectively (These are typical deposition parameters employed previously for preparation of various thin oxide films at Cardiff). Finally, Ag top electrodes were deposited on the MoO_3 layers using magnetron sputtering at a power of 1 W for 40 min. Prior to deposition, the sputtering chamber was evacuated to 9 × 10^{-4} Torr and refilled with argon gas to 5.0 × 10^{-3} Torr. During the deposition, the argon flow rate was maintained at 15 sccm and the substrate temperature was maintained at 20 °C. A mask with 4 rectangular holes of 3 mm × 5 mm (0.15 cm^2) was placed on the
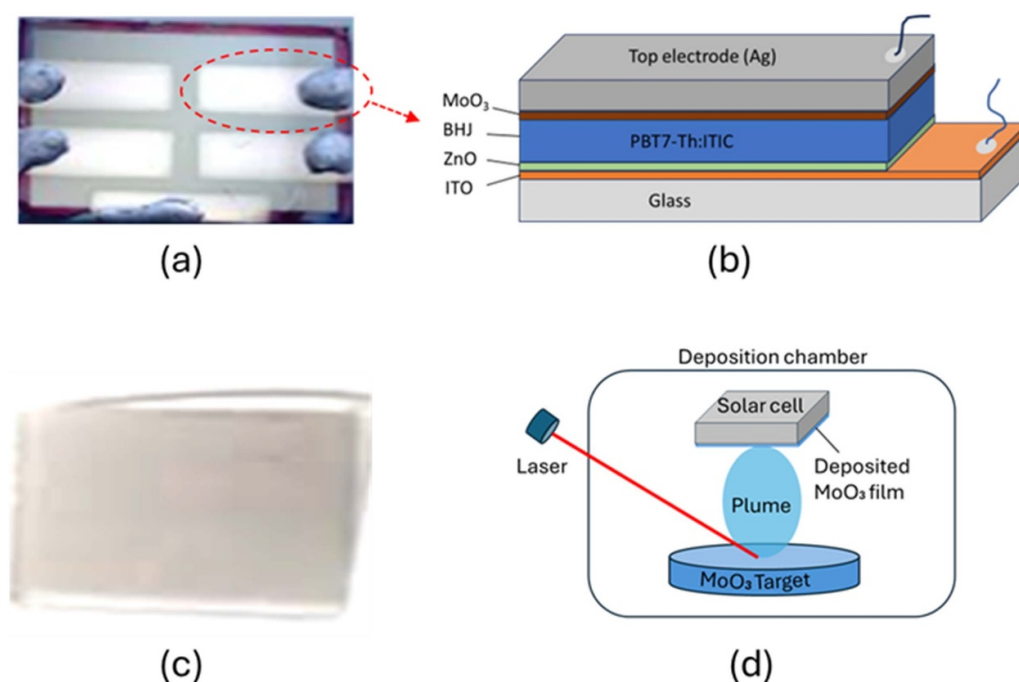
Figure 1. (a) Photograph of the organic solar cells fabricated in this study; (b) the device structure of the fabricated solar cells, consisting of five layers: ITO/ZnO/PTB7-Th:ITIC/MoO$_3$/Ag; (c) photograph of MoO$_3$ thin film on quartz glass substrate prepared using the pulsed laser deposition; (d) schematic PLD deposition of MoO$_3$ layer.

sample, which defines the Ag electrode and consequently the solar cell area (see figure 1(b)).

Characterisation: the chemical and structural properties of the fabricated films were investigated by XRD (Siemens D5000) analysis. The transmittance was determined using ultraviolet–visible spectroscopy (Hitachi U-1900), and the surface morphology was examined using an atomic force microscope (AFM, Dimension 3100). The photovoltaic performance of the solar cells was evaluated using the parameters obtained from J–V measurements, which were carried out using an Autolab *I–V* tracer (Metrohm) under one sun illumination (AM1.5, 100 mW cm^{-2}) provided by an Oriel solar simulator (LCS-100, Class ABB).

3. Results and discussion

Figure 1(a) shows a photograph of the OSCs fabricated in this study based on a device structure of ITO/ZnO/PTB7-Th:ITIC/MoO$_3$/Ag (see figure 1(b)). In this configuration, 4 identical solar cells were designed on one substrate. With the capability of processing 4 substrates in one batch, this enables 16 solar cells to be fabricated under the same conditions. Prior to studying the effect of the MoO$_3$ layer on the photovoltaic performance of the solar cells, initial experiments were performed to determine the optimal conditions for the fabrication of both ZnO and PTB7-Th:ITIC layers based on a simplified device structure of ITO/ZnO/PTB7-Th:ITIC/Ag, where the MoO$_3$ layer is absent. Another initial study was to prepare the MoO$_3$ films on the quartz substrates for determination of

the structural and optical properties of the pulsed laser deposited MoO$_3$ thin films. Figure 1(c) shows the photograph of MoO$_3$ coated quartz glass. Figure 1(d) shows the schematic PLD setup for deposition of MoO$_3$ layers.

XRD analysis was attempted to examine the chemical and structural properties of the fabricated MoO$_3$ films on quartz substrates. Figure S1 (in supplementary materials) presents the XRD patterns of the deposited MoO$_3$ films, compared to the XRD patterns of reference samples (i.e. the MoO$_3$ target and MoO$_3$ powders purchased from Sigma-Aldrich). The characteristic peaks of MoO$_3$ can be seen clearly in both reference samples. However, no corresponding peaks can be seen from the deposited MoO$_3$ samples. This is probably due to the fact that the films are too thin to produce visible peaks. Nevertheless, the presence of the deposited films is evident from UV–Vis measurements. Figure 2(a) shows the transmittances of the deposited films on quartz substrates, which are clearly lower than that of the quartz-only sample. In fact, the films can be seen visually in yellow-brownish colour (figure 1(c) and figure S2 in supplementary materials), confirming the existence of the deposited layers. In addition, the transmittance decreases with increasing the laser ablation energy, indicating an increase in the film thickness with the ablation energy. Furthermore, the optical bandgap of the deposited films can be estimated from the Tauc plots using the absorbance data from UV–Vis measurements [32]. It can be seen from figure 2(b) that the optical bandgap is approximately 3.0 eV, which is in good agreement with the published data for MoO$_3$, suggesting that films of MoO$_3$ have been deposited on the substrate. The surface morphology of
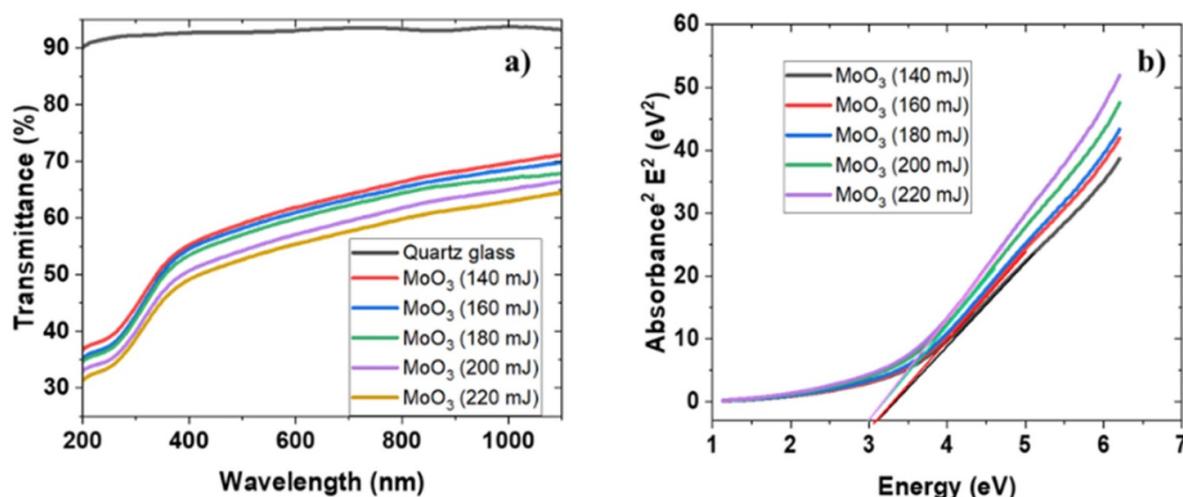
Figure 2. (a) Transmittance of the MoO_3 films on quartz substrates by pulsed laser deposition for different ablation energies, (b) the corresponding Tauc plots of MoO_3 films constructed using the measured absorbance data.
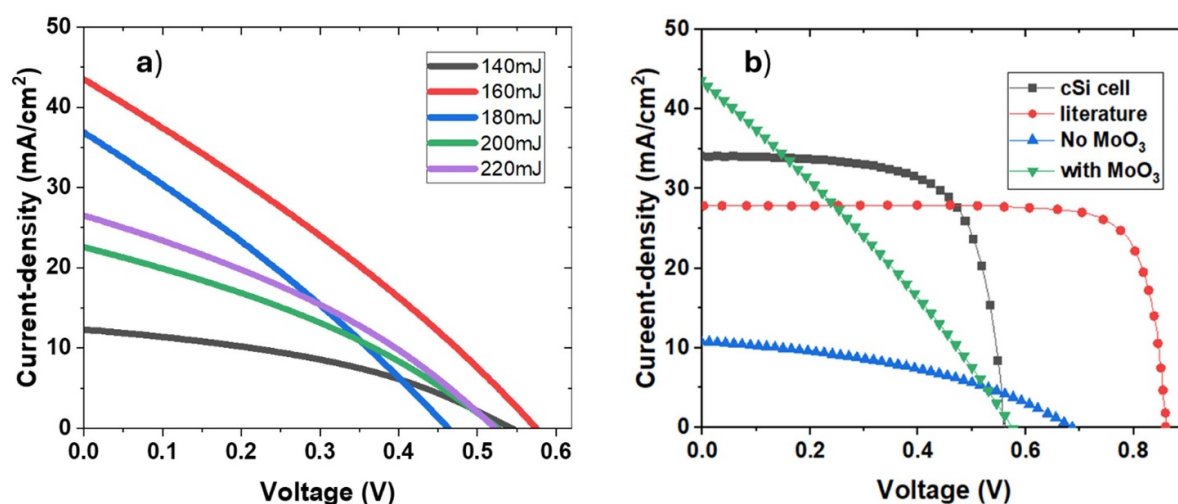

Figure 3. (a) J–V curves of the best performing devices with the MoO_3 layer deposited by PLD using different ablation energies, (b) J–V curves of a control device made from direct deposition of Ag electrode on the BHJ layer without the MoO_3 (blue), together with the published data from [6], representing the best performing organic solar cell reported to date (red) and the measured data from a commercial crystalline silicon solar cell (black). The data of the best performing devices from this work is also included (green).

the films deposited on ITO glass substrates was also examined using AFM. Compared to the ITO-only sample (figure S3 (a) in supplementary materials), the samples with the pulsed laser deposited MoO_3 show the presence of film coverage on the ITO grains (see figures S_3(b)–(f) in supplementary materials). However, the coverage appear to be incomplete, which is due to the fact that the roughness of the ITO surface is larger than the thickness of the deposited MoO_3 films. It is estimated that the maximum height between the peaks and valleys of the ITO film before MoO_3 deposition is around 30.3 nm, which reduced to between 23.4 nm and 26.7 nm after MoO_3 deposition.

The J–V curves of the fabricated devices were measured to assess the influence of the MoO_3 layers on the photovoltaic performance of the PTB7-Th:ITIC OSCs. The results of the best performing devices are shown in figure 3(a). The

photovoltaic parameters were also extracted from the measured J–V curves. The best values and the average values of the devices fabricated using different laser ablation energies are presented in table 1, where the average values were calculated from approximately 12 devices of each batch. The results show clearly that the ablation energy of the MoO_3 deposition has significant effect on the performance of the devices. The highest power conversion efficiency is obtained in the devices fabricated at an optimised ablation energy of 160 mJ, which also exhibits the largest short circuit current and open circuit voltage among all devices fabricated in this study.

The devices without the MoO_3 hole transport layer were also fabricated for comparison using the same procedures except without the PLD. The result is shown in figure 3(b), together with the data of the best performing OSCs published to date [6]. It can be seen that the devices fabricated in this

Table 1. Photovoltaic parameters of the devices with the MoO_3 layer prepared by PLD at different ablation energies, compared with a OSC that has the highest short circuit reported [6] (the 'Best' represents the data obtained from the best performing devices of the batch and the 'Average' represents the average values calculated from 8 to 13 devices of each batch. The numbers in the brackets represent the laser ablation energy employed. The row denoted 'No MoO_3' represents the control device without MoO_3 layers).

Ablation energy (mJ)	V_{oc} (V)	J_{sc} (mA cm^{-2})	FF (%)	PCE (%)	R_s (Ω.cm^2)	R_{sh} (Ω.cm^2)
Best (140)	0.54	12.31	39.08	2.6	20.2	128.9
Average (140)	0.47$\pm$ 0.07	13.51$\pm$ 2.32	31.75$\pm$ 4.50	2.1$\pm$ 0.8	24.2$\pm$ 6.7	62.9$\pm$ 29.1
Best (160)	0.57	43.59	28.72	7.2	9.4	17.4
Average (160)	0.48$\pm$ 0.09	30.41$\pm$ 7.45	29.49$\pm$ 3.67	4.3$\pm$ 1.2	14.2$\pm$ 9.0	25.9$\pm$ 13.7
Best (180)	0.46	37.00	28.36	4.8	9.8	14.9
Average (180)	0.45$\pm$ 0.03	22.38$\pm$ 8.10	29.99$\pm$ 2.14	3.0$\pm$ 0.8	15.5$\pm$ 3.7	34.2$\pm$ 14.2
Best (200)	0.52	22.62	33.08	3.9	13.7	19.6
Average (200)	0.48$\pm$ 0.03	18.82$\pm$ 8.10	31.23$\pm$ 2.10	3.0$\pm$ 0.8	18.1$\pm$ 8.2	39.9$\pm$ 8.4
Best (220)	0.52	26.58	33.17	4.6	11.4	31.5
Average (220)	0.51$\pm$ 0.03	23.20$\pm$ 1.73	31.31$\pm$ 1.65	3.8$\pm$ 0.6	14.2$\pm$ 1.3	34.4$\pm$ 4.4
Best (No MoO_3)	0.68	10.84	39.92	3.0	25.3	325.17
Average(No MoO_3)	0.63$\pm$ 0.04	10.56$\pm$ 0.84	36.80$\pm$ 4.00	2.5$\pm$ 0.6	28.0$\pm$5.0	192.0$\pm$ 67.4
REF OSC [6]	0.861	27.88	80.39	19.31	—	—

study have a smaller Voc and significantly poorer FF compared with the published data. However, the device with a MoO_3 layer exhibit a larger short-circuit current density of 43.6 mA cm^{-2}, which is more than 55% larger than the highest value reported in OSCs (27.88 mA cm^{-2} [6]). This is a surprising outcome with potentially significant impact.

To ensure the validity of measurements, J–V curves were measured in dark (see figure S4 in supplementary materials). All data points of J–V curves in dark have positive current values, confirming that the negative shift of J–V curves under light irradiation (1 sun in this case) represents the true values of the photogenerated current. Furthermore, a commercial silicon solar cell was obtained and tested under the same conditions. The measured J–V curve of the silicon solar cell is also shown in figure 3(b) for comparison. A short-circuit current density of 34.4 mA cm^{-2} is in a good agreement with the published data of typical commercial silicon solar cells [33, 34], confirming the validity of the tests. It can be seen that the highest short-circuit current obtained from this work is more than 26% larger than this silicon solar cell. This represents a remarkable increase which is rarely observed.

The fill factor (FF) is one of the important photovoltaic parameters that affects the power conversion efficiency (PCE) of solar cells. The state-of-the-art solar cells have a FF value in the range of 70%–80%. The reason for a very poor FF in the device without the MoO_3 layer can be attributed to the fact that the hole transport layer is absent in its device structure (i.e., ITO/ZnO/PTB7-Th:ITIC/Ag). In state-of-the-art OSCs, the hole transport layer is a necessity that helps to extract holes efficiently and block the electrons. This provides an easy passage for the holes to reach the Ag electrode and prevents the electrons from reaching the same electrode for recombination. Since the MoO_3 has been reported as an effective hole transport layer for OSCs [17–22], it is anticipated that the devices with a MoO_3 layer should have a larger FF than the devices without a MoO_3 layer. However, the results of this work show a completely opposite outcome that the FF is decreased with a pulsed laser deposited MoO_3 layer. The original aim of using

the MoO_3 as an effective hole transport layer has not been achieved. Instead, a substantial increase in the short-circuit current was observed. This result adds a new question to recent debates on the roles of MoO_3 layer as the hole transport layer [31]. More significantly, the result demonstrates that significantly higher short-circuit current can be achieved in OSCs. In fact, the value of 43.6 mA cm^{-2} obtained in this work is among the highest values for all types of solar cells [35].

A reduction in the FF from about 40% in the ITO/ZnO/PTB7-Th:ITIC/Ag devices to 29% in the ITO/ZnO/PTB7-Th:ITIC/MoO_3/Ag devices is detrimental to the overall efficiency of the devices. The reduction is due to a decrease in the shunt resistance from 325 Ω.cm^2 to 18 Ω.cm^2 (table 1). It is known that the shunt resistance is an indicator of electron–hole recombination. The perovskite solar cells fabricated using the same geometrical design has a shunt resistance of 9000 Ω·cm^2 [36], which corresponds to an FF of 74%. Clearly, the MoO_3 layer employed in this device failed to provide effective blocking to the electrons. Instead, it provides enhanced shunt pathways, which led to significant reduction in the FF. On the other hand, the reason for the substantial increase in the short-circuit current cannot be explained. An immediate question is if this is due to the unique properties of the 'PTB7-Th:ITIC/MoO_3' interface or associated with the use of the PLD technique. Several studies had been carried out based on the same structure (i.e. ITO/ZnO/PTB7-Th:ITIC/MoO_3/Ag) using the MoO_3 layers that were prepared using thermal evaporation [17–22]. Table 2 lists the published data of the short-circuit current density of several OSCs, compared with this work. It can be seen that the short-circuit current density of the PTB7-Th:ITIC devices is within a range of 8–17 mA cm^{-2}, which is clearly lower than the value observed in this study. Examining the key difference among these devices, we can see that the pulsed laser deposited MoO_3 layer appears to be a unique feature in the devices that exhibits the largest short-circuit current density. It is reasonable to suggest that the observed high short-circuit current density is associated with the PLD.

Table 2. Photovoltaic parameters of organic solar cells of this work compared with those of the published, together with their corresponding active layers, hole transport layers (HTL) and the methods for preparation of HTLs (PLD: pulsed laser deposition; SC: spin-coating; RF: radio frequency magnetron sputtering; TE: thermal evaporation.).

Active layer	HTL/method	J_{sc} (mA cm^{-2})	V_{oc} (V)	FF (%)	PCE (%)	References
PTB7-Th:ITIC	No HTL	10.84	0.68	39.92	3.0	This work
PTB7-Th:ITIC	MoO$_3$/PLD	43.59	0.57	28.72	7.2	This work
P3HT:PCBM	MoO$_3$/SC	8.36	0.64	59.0	3.14	[23]
P3HT: PCBM	MoO$_3$/RF	9.50	0.574	60.0	3.27	[26]
PTB7-Th:ITIC	MoO$_3$/TE	13.8	0.83	60.0	6.84	[21]
PTB7-Th:ITIC	MoO$_3$/TE	14.3	0.84	60.6	7.4	[20]
PTB7-Th:ITIC	MoO$_3$/TE	16.47	0.685	70.5	7.91	[12]
PTB7-Th:ITIC	MoO$_3$/TE	17.0	0.758	61.9	7.98	[22]
PBDTTS-TClQx:Y6	PDINO/SC	25.9	0.81	67.53	14.28	[39]
PM6:BTP-eC9,TCB	MoO$_3$/TE	27.88	0.861	80.39	19.31	[6]

The PLD process results in a plasma of energetic particles making contact with the top layer of the substrate. Such a feature may produce a unique interaction between the MoO$_3$ and the photoactive layer. MoO$_3$ has been shown to be a p-type dopant for semiconducting polymers, resulting in an increase in current density of the doped polymer [37, 38]. Based on these findings, we speculate that energetic MoO$_3$ particles from the laser ablation may be implanted into the photoactive layer, leading to a transformation of photo-absorption behaviour in the PTB7-Th:ITIC layer and consequently a significant improvement in charge generation of the photoactive layer. However, it should be noted that this is a pure speculation. Further investigations are needed to identify the exact mechanisms responsible for such substantial improvement.

4. Conclusions

A considerably high short-circuit current density of 43.9 mA cm^{-2} was obtained in OSCs that have a device structure of ITO/ZnO/PTB7-Th:ITIC/MoO$_3$/Ag with the MoO$_3$ layers fabricated using PLD. This value is approximately 55% higher than the highest value reported to date in OSCs. A comparative study was carried out using the devices that were fabricated based on a similar device structure but without the MoO$_3$ layer (i.e. ITO/ZnO/PTB7-Th:ITIC/Ag). This result, together with the published data from the same type of devices with the MoO$_3$ layer fabricated using vacuum thermal evaporation, indicates that the observed increase in the short-circuit current is associated with the use of the PLD technique for the fabrication of MoO$_3$ layer. The exact mechanisms responsible for the observed increase is yet to be identified and further investigation is needed. The result reported here provides experimental evidence that higher short-circuit current density could also be achieved in OSCs. It should be noted that this high current density is achieved at the expense of a significantly reduced fill factor. As a result, the power conversion efficiency of these solar cells are still very low. To fully benefit from the increased short-circuit current density, the problem of the accompanied reduction in the fill factor must be resolved. Further investigations are needed

to identify the mechanisms that led to high short-circuit current, as well as understand the causes of reduction in the fill factor.

Conflict of interest

The authors declare no conflict of interest.

Author contributions

Godwin N Ugwuanyi ⓘ 0000-0003-2871-0509
Conceptualization (lead), Data curation (lead), Formal analysis (lead), Funding acquisition (lead), Investigation (lead), Methodology (lead), Validation (equal), Visualization (lead), Writing – original draft (supporting), Writing – review & editing (supporting)

Martin C Eze ⓘ 0000-0003-2724-7516
Data curation (supporting), Formal analysis (supporting), Investigation (supporting), Methodology (supporting), Validation (supporting), Visualization (supporting), Writing – review & editing (supporting)

Sukhwinder Singh 0000-0002-4788-8292
Data curation (supporting), Formal analysis (supporting),
Investigation (supporting), Writing – review &
editing (supporting)

Hamed Ifheema
Data curation (supporting), Investigation (supporting)

Victoria G Rocha 0000-0001-6125-8556
Methodology (supporting), Supervision (supporting),
Validation (supporting), Writing – review &
editing (supporting)

Bo Hou 0000-0001-9918-8223
Formal analysis (supporting), Investigation (supporting),
Methodology (supporting), Supervision (supporting),
Validation (supporting), Writing – review &
editing (supporting)

Gao Min 0000-0001-9591-5825
Formal analysis (equal), Funding acquisition (lead),
Investigation (supporting), Methodology (equal), Project
administration (lead), Resources (lead), Supervision (lead),
Validation (supporting), Visualization (supporting), Writing –
original draft (lead), Writing – review & editing (lead)

References

[1] Heeger A J 2014 25th anniversary article: bulk heterojunction solar cells: understanding the mechanism of operation *Adv. Mater.* **26** 10–28

[2] Tang C W 1986 Two layer organic photovoltaic cell *Appl. Phys. Lett.* **48** 183–185

[3] Park S H, Roy A, Beaupré S, Cho S, Coates N, Moon J S, Moses D, Leclerc M, Lee K and Heeger A J 2009 Bulk heterojunction solar cells with internal quantum efficiency approaching 100% *Nat. Photon.* **3** 297–303

[4] Sariciftci N S, Smilowitz L, Heeger A J and Wudl F 1992 Photoinduced electron transfer from a conducting polymer to buckminsterfullerene *Science* **258** 1474

[5] Lin Y *et al* 2015 An electron acceptor challenging fullerene for efficient polymer solar cells *Adv. Mater.* **27** 1170–4

[6] Fu J *et al* 2023 19.31% binary organic solar cell and low nonradiative recombination enabled by nonmonotonic intermediate state transition *Nat. Commun.* **14** 1760

[7] Gurney R S, Lidzey D G and Wang T 2019 A review of non-fullerene polymer solar cells: from device physics to morphology control *Rep. Prog. Phys.* **82** 036601

[8] Xiao B, Zhao Y, Tang A, Wang H, Yang J and Zhou E 2017 PTB7-Th based organic solar cell with a high Voc of 1.05 V by modulating the LUMO energy level of benzotriazole-containing non-fullerene acceptor *Sci. Bull.* **62** 1275–82

[9] Alghamdi A R, Kirk B P, Andersson M R and Andersson G G 2023 Chemical and electronic properties of PTB7-Th and ITIC on ZnO interfaces in organic solar cells *ACS Sustain. Chem. Eng.* **11** 11811–8

[10] Alghamdi A R, Kirk B P, Kocak G, Andersson M R and Andersson G G 2022 Modification of the surface composition of PTB7-Th: ITIC blend using an additive *Molecules* **27** 6358

[11] Tang Y, Liu L, Deng J, Sun P, Yan D, Peng W, Huang X, Xiao M, Tao Q and Yu D 2023 Incorporating a weak acceptor unit into PTB7-Th to tune the open circuit voltage for non-fullerene polymer solar cells *Tetrahedron* **131** 133214

[12] Jia B, Dai S, Ke Z, Yan C, Ma W and Zhan X 2018 Breaking 10% efficiency in semitransparent solar cells with fused-undecacyclic electron acceptor *Chem. Mater.* **30** 239–45

[13] Bai S *et al* 2012 Inverted organic solar cells based on aqueous processed ZnO interlayers at low temperature *Appl. Phys. Lett.* **100** 4719201

[14] Liu C, Xiao C and Li W 2021 Zinc oxide nanoparticles as electron transporting interlayer in organic solar cells *J. Mater. Chem. C* **9** 14093–114

[15] Jiang P *et al* 2022 Precursor engineering to reduce processing temperature of ZnO films for flexible organic solar cells *Angew. Chem.—Int. Ed.* **61** 202208815

[16] Meyer J, Hamwi S, Kröger M, Kowalsky W, Riedl T and Kahn A 2012 Transition metal oxides for organic electronics: energetics, device physics and applications *Adv. Mater.* **24** 5408–27

[17] Shrotriya V, Li G, Yao Y, Chu C-W and Yang Y 2006 Transition metal oxides as the buffer layer for polymer photovoltaic cells *Appl. Phys. Lett.* **88** 073508

[18] Wang Y, Wu B, Wu Z, Lan Z, Li Y, Zhang M and Zhu F 2017 Origin of efficient inverted nonfullerene organic solar cells: enhancement of charge extraction and suppression of bimolecular recombination enabled by augmented internal electric field *J. Phys. Chem. Lett.* **8** 5264–71

[19] Yi X *et al* 2018 Impact of nonfullerene molecular architecture on charge generation, transport, and morphology in PTB7-Th-Based organic solar cells *Adv. Funct. Mater.* **28** 1820702

[20] Duan L, Yi H, Zhang Y, Haque F, Xu C and Uddin A 2019 Comparative study of light and thermal induced degradation for both fullerene and non-fullerene-based organic solar cells *Sustain. Energy Fuels* **3** 723–5

[21] Lin H, Yang L, Chen Q, Kong X, Du X, Zhao W, Wang Z, Zheng C, Tao S and Tong Q 2020 An universal morphology regulator for efficient and stable nonfullerene organic solar cells by π–π interaction *Org. Electron.* **86** 105827

[22] Li T, Dai S, Ke Z, Yang L, Wang J, Yan C, Ma W and Zhan X 2018 Fused tris(thienothiophene)-based electron acceptor with strong near-infrared absorption for high-performance as-cast solar cells *Adv. Mater.* **30** 1705969

[23] Liu F, Shao S, Guo X, Zhao Y and Xie Z 2010 Efficient polymer photovoltaic cells using solution processed MoO₃ as anode buffer layer *Sol. Energy Mater. Sol. Cells* **94** 842–5

[24] Girotto C, Voroshazi E, Cheyns D, Heremans P and Rand B P 2011 Solution-processed MoO₃ thin films as a hole-Injection layer for organic solar cells *ACS Appl. Mater. Interfaces* **3** 3244–7

[25] Gesheva K A and Ivanova T A 2006 Low-temperature atmospheric pressure CVD process for growing thin films of MoO₃ and MoO₃-WO₃ for electrochromic device applications *Chem. Vap. Depos.* **12** 231–8

[26] Fan X, Fang G, Qin P, Sun N, Liu N, Zheng Q, Cheng F, Yuan L and Zhao X 2011 Deposition temperature effect of RF magnetron sputtered molybdenum oxide films on the power conversion efficiency of bulk-heterojunction solar cells *J. Phys. D: Appl. Phys.* **44** 045101

[27] Ramana C V and Julien C M 2006 Chemical and electrochemical properties of molybdenum oxide thin films prepared by reactive pulsed-laser assisted deposition *Chem. Phys. Lett.* **428** 114–8

[28] Holovský J, Horynová E, Horák L, Ridzoňová K, Remeš Z, Landová L and Sharma R K 2021 Pulsed laser deposition of high-transparency molybdenum oxide thin films *Vacuum* **194** 110613

[29] Kuppusami P and Raghunathan V S 2006 Status of pulsed laser deposition: challenges and opportunities *Surf. Eng.* **22** 81–83

[30] Shepelin N A, Tehrani Z P, Ohannessian N, Schneider C W, Pergolesi D and Lippert T 2023 A practical guide to pulsed laser deposition *Chem. Soc. Rev.* **52** 2294–321

[31] Meyer J 2011 Electronic structure of molybdenum-oxide films and associated charge injection mechanisms in organic devices *J. Photon. Energy* **1** 011109–1

[32] Tauc J 1968 Optical properties and electronic structure of amorphous Ge and Si *Mater. Res. Bull.* **3** 37–46

[33] Honsberg C and Bowden S 2019 Short-Circuit Current (available at: www.pveducation.org/pvcdrom/solar-cell-operation/short-circuit-current) (Accessed 26 October 2025)

[34] Wehra G, Zanescoa I and Moehleckea A 2019 Influence of diffusion parameters on electrical characteristics of mc-si solar cells with aluminum and phosphorus diffusion performed in the same thermal step *Mater. Res.* **22** 20180443

[35] Green M A, Hishikawa Y, Dunlop E D, Levi D H, Hohl-Ebinger J and Ho-Baillie A W Y 2018 Solar cell efficiency tables (version 52) *Prog. Photovolt., Res. Appl.* **26** 427–36

[36] Eze M C, Ugwuanyi G, Li M, Eze H U, Rodriguez G M, Evans A, Rocha V G, Li Z and Min G 2021 Optimum silver contact sputtering parameters for efficient perovskite solar cell fabrication *Sol. Energy Mater. Sol. Cells* **230** 111185

[37] Zhang J *et al* 2017 Study of molybdenum trioxide as a p-type dopant in organic semiconductors: the influence of density of gap states on their n-/p type characteristics *Adv. Eng. Res.* **114** 609–14

[38] Yang J, Wang X, Yu X, Liu J, Zhang Z, Zhong J and Yu J 2023 Improved short-circuit current and fill factor in PM6:Y6 organic solar cells through D18-Cl doping *Nanomaterials* **13** 2899

[39] Zhou Z, Xu Y, Yang J, Jin S, Zhao Y, Zhu W and Liu Y 2024 High-performance nonfullerene polymer solar cells based on chlorinated quinoxaline copolymer with a high short-circuit current density *Org. Electron.* **127** 107004